

Transport Signatures of Radial Rashba Spin-Orbit Coupling at Ferromagnet/Superconductor Interfaces

Andreas Costa^{1,*} and Jaroslav Fabian¹

¹*Institute for Theoretical Physics, University of Regensburg, 93040 Regensburg, Germany*

(Dated: December 6, 2024)

Spin-orbit coupling (SOC) emerging at the interfaces of superconducting magnetic tunnel junctions is at the heart of multiple unprecedented physical phenomena, covering triplet proximity effects induced by unconventional (spin-flip) Andreev reflections, giant transport magnetoanisotropies, sizable tunneling anomalous Hall effects, and electrically controlled current-reversing $0-\pi$ (like) transitions in Josephson contacts. Recent first-principles calculations proposed that the Rashba spin-orbit fields in twisted graphene/transition-metal dichalcogenide and van-der-Waals multilayers can—owing to broken mirror symmetries—exhibit an unconventional radial component (with spin parallel to the electron’s momentum), which can be quantified by the Rashba angle θ_R . We theoretically explore the ramifications of radial Rashba SOC at the interfaces of vertical ferromagnet/superconductor tunnel junctions with a focus on the magnetoanisotropies of the tunneling and tunneling-anomalous-Hall-effect conductances. Our results demonstrate that θ_R can be experimentally extracted from respective magnetization-angle shifts, providing a practical way to probe the radial Rashba SOC induced by twisted multilayers that are placed as tunneling barrier between ferromagnetic and superconducting electrodes.

I. INTRODUCTION

Spin-orbit coupling (SOC) is essential for electrically manipulating electron spins in spintronics devices [1, 2]. Tunnel junctions that consist of different-material electrodes are particularly interesting to explore [3–7], as their inherently broken space-inversion symmetry induces strong interfacial Rashba SOC [8, 9]. If the tunneling barriers furthermore lack bulk-inversion symmetry—like, e.g., zincblende semiconductors [10]—the Rashba spin-orbit fields interfere with additionally emerging spin-orbit fields of the Dresselhaus type [11], and unique transport features such as the C_{2v} -symmetric tunneling anisotropic magnetoresistance (TAMR) effect [3, 12]—referring to in-plane tunneling-conductance magnetoanisotropies—or the tunneling anomalous Hall effect (TAHE) [4, 13] appear.

Two-dimensional materials and van-der-Waals multilayer structures are attracting enormous research interest [14–18], as many of their physical properties can be engineered exploiting knobs such as the number of monolayers, stacking order, twisting, or gating [19–29]. Proximitizing graphene by transition-metal dichalcogenides was, for example, predicted to induce novel Ising-like valley–Zeeman SOC that results in giant spin-relaxation anisotropies [30–33]. The broken space inversion in graphene/transition-metal dichalcogenide and van-der-Waals multilayers likewise generates Rashba spin-orbit fields. Pioneering first-principles studies proposed that breaking mirror symmetries by twisting the monolayers can—apart from the conventional Rashba (CR) with a spin texture that is perpendicular to the electron momentum—imprint a (purely) unconventional radial Rashba (RR) component, which prefers a spin alignment parallel to the momentum, on the Rashba spin-orbit field [20, 21, 34, 35]; the ratio between CR and RR SOC is quantified by the Rashba angle θ_R ($\theta_R = 0$ indicates CR SOC, $\theta_R = 0.5\pi$ RR SOC, and $0 < \theta_R < 0.5\pi$ an admixture of both).

Extremely rich physics is bound to occur when SOC interacts with ferromagnetism and superconducting coherence [36, 37]. Among the perhaps most striking phenomena are unconventional spin-flip Andreev reflections that induce superconducting triplet correlations in proximitized regions [36, 38–44] and lead to marked transport anomalies, such as remarkably enhanced conductance magnetoanisotropies [5–7, 45, 46]—termed magnetoanisotropic Andreev reflection (MAAR)—or sizable superconducting TAHEs [47], as well as the recently intensively investigated supercurrent diode effect [48–60].

In Ref. [59], the authors performed numerical transport calculations for lateral graphene-based van-der-Waals heterostructures and identified robust magnetotransport signatures to disentangle CR and RR SOC in experiments. Furthermore, Ref. [61] reported the interplay of crossed CR and RR SOC at the interfaces of highly-ballistic superconductor/ferromagnet/superconductor Josephson junctions predicting the emergence of the so-called *unconventional supercurrent diode effect*. Contrary to the well-studied conventional supercurrent diode effect, which typically originates from a finite center-of-mass momentum that an in-plane magnetic field aligned *perpendicular to the current* imprints on the Cooper pairs [53, 62–66], the unconventional supercurrent diode effect only occurs when the magnetization of the ferromagnet has a nonzero component perpendicular to the plane of the SOC, i.e., *parallel to the current*. We unraveled that the spins of the current-carrying electrons are initially polarized in the plane by the spin-orbit field at the left junction interface, travel afterwards through the ferromagnet and precess in this plane around the axis defined by the perpendicular magnetization, and then arrive at the right interface at which they see the second spin-orbit field rotated by an effective angle determining the transmission probability into the second superconductor. If both SOC are functionally different (i.e., they are described by different Rashba angles), the rotation angles—and therefore the transmission probabilities—are different for left- and right-propagating electrons, resulting in polarity-dependent critical currents and hence in the unconventional supercurrent diode effect.

* Corresponding author: andreas.costa@physik.uni-regensburg.de

In this article, we address the yet unexplored ramifications of RR SOC induced at the interface of highly-ballistic vertical ferromagnet/superconductor junctions on the corresponding tunneling-transport (and thereby microscopically on the Andreev tunneling) and TAHE characteristics with a focus on identifying experimental signatures to determine the Rashba angle θ_R . We will demonstrate that the presence of unconventional RR spin-orbit fields can be probed through the in-plane magnetoanisotropies of the TAHE conductances and Hall supercurrent responses that will both reflect magnetization-angle shifts proportional to θ_R (in agreement with the general symmetry analysis provided in Ref. [59]), or similarly also from the in-plane tunneling-conductance magnetoanisotropies (i.e., from the in-plane MAAR) when RR interferes with a functionally distinct spin-orbit field like, for instance, Dresselhaus SOC.

The paper is organized in the following way. In Sec. II, we introduce the theoretical model that we apply to compute the tunneling and TAHE conductances and that is kept most general to allow for the simultaneous presence of CR, RR, and Dresselhaus SOC at the ferromagnet/superconductor junction interface, as well as for arbitrary magnetization directions and bias voltages. We discuss and analyze our numerical results at zero bias in Sec. III, unraveling the θ_R -dependent magnetization-angle shifts as clear transport fingerprints of RR SOC. Our findings are summarized in Sec. IV, while Appendix A contains additional technical details to calculate the Hall supercurrent responses on the superconducting side of the junction.

II. THEORETICAL MODEL

We consider an epitaxial, highly-ballistic, three-dimensional F/B/S tunnel junction, in which the two semi-infinite ferromagnetic (F; spanning $z < 0$) and superconducting (S; spanning $z > 0$) regions are connected by an ultrathin tunneling barrier (B) at $z = 0$; see Fig. 1(e). Additionally to potential scattering, the barrier breaks space-inversion symmetry and induces interfacial SOC. Generalizing earlier works [5–7, 47], we assume that the corresponding Rashba spin-orbit field can acquire an additional RR component, whose ratio w.r.t. the CR SOC is determined by the Rashba angle θ_R . A possible experimental realization of the RR SOC could, for example, exploit a twisted van-der-Waals bilayer as tunneling barrier.

To model the junction, we start from its stationary Bogoljubov–de Gennes (BdG) Hamiltonian [67]

$$\hat{\mathcal{H}}_{\text{BdG}} = \begin{bmatrix} \hat{\mathcal{H}}_e & \hat{\Delta}_S(z) \\ \hat{\Delta}_S^\dagger(z) & \hat{\mathcal{H}}_h \end{bmatrix}, \quad (1)$$

where $\hat{\mathcal{H}}_e = [-\hbar^2/(2m)\nabla^2 - \mu]\hat{\sigma}_0 - (\Delta_{\text{XC}}/2)\Theta(-z)(\hat{\mathbf{m}} \cdot \hat{\boldsymbol{\sigma}}) + \hat{\mathcal{H}}_B$ refers to the single-electron Hamiltonian and $\hat{\mathcal{H}}_h = -\hat{\sigma}_y \hat{\mathcal{H}}_e^* \hat{\sigma}_y$ to its hole counterpart; $\hat{\sigma}_0$ ($\hat{\sigma}_i$) is the 2×2 identity (i th Pauli spin) matrix and $\hat{\boldsymbol{\sigma}} = [\hat{\sigma}_x, \hat{\sigma}_y, \hat{\sigma}_z]^T$. The magnetization direction in the ferromagnet is given by the unit vector $\hat{\mathbf{m}} = [\sin(\Theta)\cos(\Phi), \sin(\Theta)\sin(\Phi), \cos(\Theta)]^T$ —where the polar angle Θ is measured w.r.t. the out-of-plane $\hat{z} \parallel [001]$ -

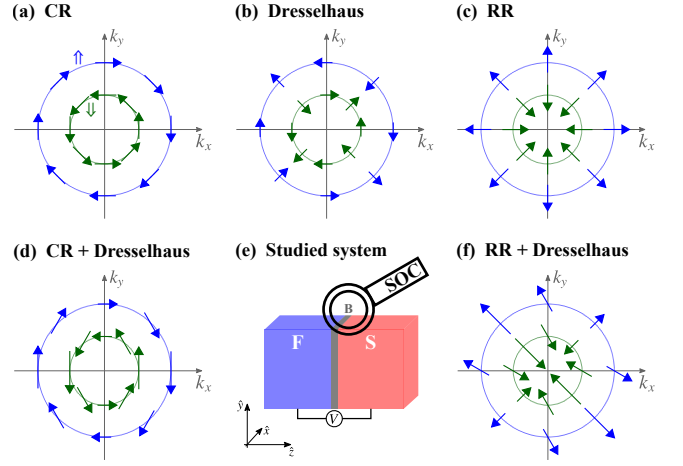


FIG. 1. Illustration of the \mathbf{k} -space representation of the spin-orbit fields at the tunneling-barrier interface along the SOC-split spin-up (\uparrow ; blue) and spin-down (\downarrow ; dark-green) Fermi surfaces, defining the preferred in-plane spin orientation, for (a) CR, (b) (weak) Dresselhaus, and (c) RR SOC. Interference of Dresselhaus with CR or RR SOC results in the spin-orbit fields depicted in (d) and (f). (e) Schematic sketch of the considered three-dimensional F/B/S junction using C_{2v} principal crystallographic orientations $\hat{x} \parallel [110]$, $\hat{y} \parallel [\bar{1}10]$, and $\hat{z} \parallel [001]$.

axis and the azimuthal angle Φ w.r.t. the in-plane $\hat{x} \parallel [110]$ -reference axis—and its exchange splitting is denoted by Δ_{XC} . The ultrathin barrier is described in a deltalike manner as $\hat{\mathcal{H}}_B = [V_B d_B \hat{\sigma}_0 + \hat{\boldsymbol{\Omega}}(k_x, k_y) \cdot \hat{\boldsymbol{\sigma}}]\delta(z)$, accounting for the barrier height (width) V_B (d_B) and the in-plane spin-orbit field

$$\hat{\boldsymbol{\Omega}}(k_x, k_y) = \begin{bmatrix} \alpha[\sin(\theta_R)k_x + \cos(\theta_R)k_y] - \beta k_y, \\ \alpha[-\cos(\theta_R)k_x + \sin(\theta_R)k_y] - \beta k_x, 0 \end{bmatrix} \quad (2)$$

with general Rashba SOC, quantified by its strength α and Rashba angle θ_R , and linearized Dresselhaus SOC parameterized by β . Note that $\theta_R = 0$ corresponds to CR SOC [see Fig. 1(a)], while $\theta_R = 0.5\pi$ represents the unconventional RR SOC [see Fig. 1(c)]. We additionally include weak Dresselhaus SOC (assuming $\beta \ll \alpha$) into our model [see Fig. 1(b)], which could—even in barriers that intrinsically preserve bulk-inversion symmetry—be induced by straining [68] and will be crucial to discern RR from CR SOC in tunneling-transport data (see Sec. III). As discussed in Ref. [69], we approximate the superconducting pairing potential by $\hat{\Delta}_S(z) = \Delta_0 \Theta(z) \hat{\sigma}_0$ with the zero-temperature superconducting gap Δ_0 . We furthermore consider same Fermi levels μ and effective masses m throughout the junction to simplify the analytical treatment.

Since the in-plane wave vector $\mathbf{k}_{\parallel} = [k_x, k_y, 0]^T$ is conserved, the solutions of the BdG equation $\hat{\mathcal{H}}_{\text{BdG}}\Psi^\sigma(\mathbf{r}) = E\Psi^\sigma(\mathbf{r})$, where $\mathbf{r} = [\mathbf{r}_{\parallel}, z]^T = [x, y, z]^T$, factorize into $\Psi^\sigma(\mathbf{r}) = \psi^\sigma(z) e^{i(\mathbf{k}_{\parallel} \cdot \mathbf{r}_{\parallel})}$. The wave functions $\psi^\sigma(z)$ for the effectively remaining, single-channel, scattering problem perpendicular to the junction interface for incoming electrons with spin $\sigma = (-)1$, indicating a spin (antiparallel) parallel to $\hat{\mathbf{m}}$,

read as

$$\begin{aligned} \psi^\sigma(z < 0) = & e^{ik_e^\sigma z} \chi_e^\sigma + r_e^{\sigma,\sigma} e^{-ik_e^\sigma z} \chi_e^\sigma + r_e^{\sigma,-\sigma} e^{-ik_e^\sigma z} \chi_e^{-\sigma} \\ & + r_h^{\sigma,-\sigma} e^{ik_h^\sigma z} \chi_h^{-\sigma} + r_h^{\sigma,\sigma} e^{ik_h^\sigma z} \chi_h^\sigma \end{aligned} \quad (3)$$

in the ferromagnet and

$$\begin{aligned} \psi^\sigma(z > 0) = & t_e^{\sigma,\sigma} e^{iq_e z} [u, 0, v, 0]^\top + t_e^{\sigma,-\sigma} e^{iq_e z} [0, u, 0, v]^\top \\ & + t_h^{\sigma,\sigma} e^{-iq_h z} [v, 0, u, 0]^\top + t_h^{\sigma,-\sigma} e^{-iq_h z} [0, v, 0, u]^\top \end{aligned} \quad (4)$$

in the superconductor. The spinors for spin- σ electrons and holes in the ferromagnet are

$$\chi_e^\sigma = [\sigma\sqrt{1 + \sigma \cos(\Theta)} e^{-i\Phi}, \sqrt{1 - \sigma \cos(\Theta)}, 0, 0]^\top / \sqrt{2} \quad (5)$$

and

$$\chi_h^\sigma = [0, 0, -\sigma\sqrt{1 - \sigma \cos(\Theta)} e^{-i\Phi}, \sqrt{1 + \sigma \cos(\Theta)}]^\top / \sqrt{2}, \quad (6)$$

respectively, while the Bardeen–Cooper–Schrieffer coherence factors in the superconductor at excitation energy $E > 0$ fulfill

$$u^2 = \frac{1}{2} \left(1 + \frac{\sqrt{E^2 - \Delta_0^2}}{E} \right) = 1 - v^2 \quad (7)$$

Within Andreev approximation, we assume that $E, \Delta_0 \ll \mu$ to approximate the electron(like) and hole(like) wave vectors as

$$k_e^\sigma \approx k_h^\sigma \approx \sqrt{k_F^2 (1 + \sigma P) - \mathbf{k}_\parallel^2} \quad (8)$$

in the ferromagnet and

$$q_e \approx q_h \approx \sqrt{k_F^2 - \mathbf{k}_\parallel^2} \quad (9)$$

in the superconductor; $P = (\Delta_{XC}/2)/\mu$ is a measure for the spin polarization of the ferromagnet and $k_F = \sqrt{2m\mu}/\hbar$ denotes the Fermi wave vector.

The energy-dependent scattering coefficients $r_e^{\sigma,(-)\sigma}(E)$, $r_h^{\sigma,(-)\sigma}(E)$, and $t_{e[h]}^{\sigma,(-)\sigma}(E)$ —corresponding to (spin-flip) spin-conserving specular reflections, (spin-conserving) spin-flip Andreev reflections, and (spin-flip) spin-conserving electronlike [holelike] transmissions—are obtained applying the interfacial (at $z = 0$) boundary conditions

$$\psi^\sigma(z = 0_-) = \psi^\sigma(z = 0_+) \quad (10)$$

and

$$\begin{aligned} \left\{ \left[\frac{\hbar^2}{2m} \frac{d}{dz} + V_B d_B \right] \right\} \hat{\eta} \psi^\sigma(z)|_{z=0_-} \\ + \left[\begin{array}{cc} \hat{\Omega} \cdot \hat{\sigma} & \hat{0}_{2 \times 2} \\ \hat{0}_{2 \times 2} & -(\hat{\Omega} \cdot \hat{\sigma}) \end{array} \right] \psi^\sigma(z)|_{z=0_-} \\ = \frac{\hbar^2}{2m} \frac{d}{dz} \hat{\eta} \psi^\sigma(z)|_{z=0_+} \end{aligned} \quad (11)$$

to the scattering states in Eqs. (3)–(4), and numerically solving the resulting system of equations ($\hat{\eta} = \text{diag}[\hat{\sigma}_0, -\hat{\sigma}_0]$).

Generalizing the Blonder–Tinkham–Klapwijk approach [70], the differential tunneling conductance at zero temperature is then evaluated from

$$G_z = \frac{dI_z}{dV} = \frac{G_S}{2\pi k_F^2} \sum_\sigma \int d^2 \mathbf{k}_\parallel \left\{ 1 - \Re \left[|r_e^{\sigma,\sigma}(eV)|^2 + \frac{k_e^{-\sigma}}{k_e^\sigma} |r_e^{\sigma,-\sigma}(eV)|^2 \right] + \Re \left[\frac{k_h^{-\sigma}}{k_e^\sigma} |r_h^{\sigma,-\sigma}(-eV)|^2 + \frac{k_h^\sigma}{k_e^\sigma} |r_h^{\sigma,\sigma}(-eV)|^2 \right] \right\} \quad (12)$$

and the transverse TAHE conductances (computed in the ferromagnet close to the interface) from [47]

$$G_{x(y)} = \frac{dI_{x(y)}}{dV} = -\frac{G_S}{2\pi k_F^2} \sum_\sigma \int d^2 \mathbf{k}_\parallel \frac{k_{x(y)}}{k_e^\sigma} \left\{ \Re \left[|r_e^{\sigma,\sigma}(eV)|^2 + |r_e^{\sigma,-\sigma}(eV)|^2 \right] + \Re \left[|r_h^{\sigma,-\sigma}(-eV)|^2 + |r_h^{\sigma,\sigma}(-eV)|^2 \right] \right\}; \quad (13)$$

$G_S = Ae^2 k_F^2 / (2\pi h)$ denotes Sharvin's conductance of a perfectly transparent three-dimensional point contact (e is the positive elementary charge) [71], while taking the real parts $\Re(\dots)$ ensures to only include propagating modes. The transverse supercurrent responses $J_{x(y)}$ in the superconductor are computed from Green's functions analogously to Ref. [72]. The technical details are summarized in Appendix A.

III. RESULTS

To analyze the ramifications of RR SOC on superconducting transport, we numerically evaluate the tunneling and TAHE conductances by means of Eqs. (12) and (13) for realistic parameters. The spin polarization of the ferromagnet is set to $P = (\Delta_{XC}/2)/\mu = 0.4$, which corresponds to a weak ferro-

magnet (for iron, $P = 0.7$), while the tunneling barrier is characterized by the dimensionless Blonder–Tinkham–Klapwijk Z -parameter [70] $Z = 2mV_B d_B / (\hbar^2 k_F) = 1$, suggesting a high interfacial transparency of about $\tau = [1 + (Z/2)^2]^{-1} = 80\%$; Rashba SOC $\lambda_R = 2m\alpha/\hbar^2 = 1$ is the dominant SOC (Dresselhaus SOC is $\lambda_D = 2m\beta/\hbar^2 = 0.1$ in Fig. 3, tuned in Fig. 6, and absent otherwise) and we focus, for simplicity, on the zero-bias

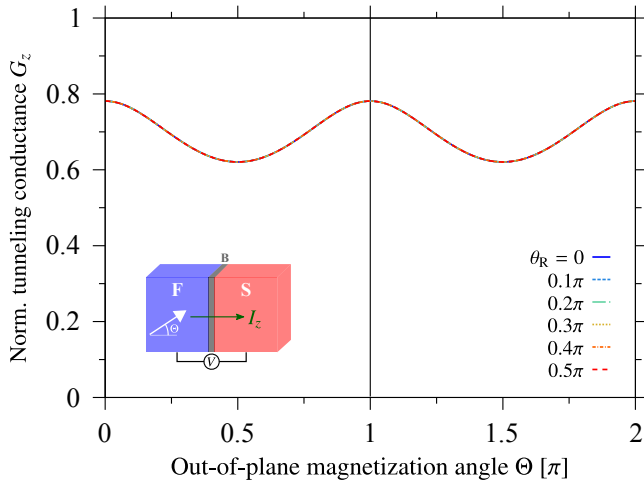


FIG. 2. Calculated dependence of the tunneling conductance $G_z = dI_z/dV$ —normalized to Sharvin’s conductance $G_S = Ae^2k_F^2/(2\pi h)$ —on the out-of-plane magnetization angle Θ for various indicated Rashba angles $\theta_R \in [0; 0.5\pi]$; the Rashba SOC parameter is $\lambda_R = 2m\alpha/\hbar^2 = 1$ and Dresselhaus SOC is absent.

regime ($eV = 0$).

A. Magnetoanisotropic Tunneling Transport

Tunneling magnetoanisotropies are among the most commonly used transport measures to probe interfacial SOC [12, 46]. If only Rashba SOC is present, the in-plane magnetoanisotropy will disappear due to the in-plane invariance of the Rashba field, whereas the out-of-plane magnetoanisotropy will be finite and originate from a SOC-induced energy splitting of the ferromagnet’s spin subbands [3]. As this splitting is proportional to the strength α of the Rashba SOC [73] only, but independent of the Rashba angle θ_R , we predict that CR and RR SOC’s cannot be disentangled from out-of-plane magnetoanisotropy measurements. Our model calculations presented in Fig. 2 indeed confirm this expected θ_R -invariance of the out-of-plane magnetoanisotropy.

To distinguish between CR and RR SOC’s from tunneling transport, we therefore need to focus on in-plane magnetoanisotropies (indicating $\Theta = 0.5\pi$) in the simultaneous presence of Rashba and Dresselhaus SOC’s; Dresselhaus SOC has not yet been conclusively identified in twisted van-der-Waals materials but a small contribution could emerge, e.g., from straining at multilayer interfaces [68]. For our calculations, we assume a hypothetical Dresselhaus SOC that is ten-times weaker than the Rashba SOC, i.e., $\lambda_D = 2m\beta/\hbar^2 = 0.1 \ll \lambda_R$. The dependence of the tunneling conductance G_z on the in-plane magnetization angle Φ in the ferromagnet is illustrated for different Rashba angles $\theta_R \in [0; 0.5\pi]$ in Fig. 3(a). As analyzed in Ref. [5], spin-flip Andreev reflections are the main source of transport magnetoanisotropies at subgap bias voltages. The conductance contribution of these spin-flip Andreev reflections is maximal whenever the interfacial spin-orbit fields favor an in-plane spin orientation that is perpendicular

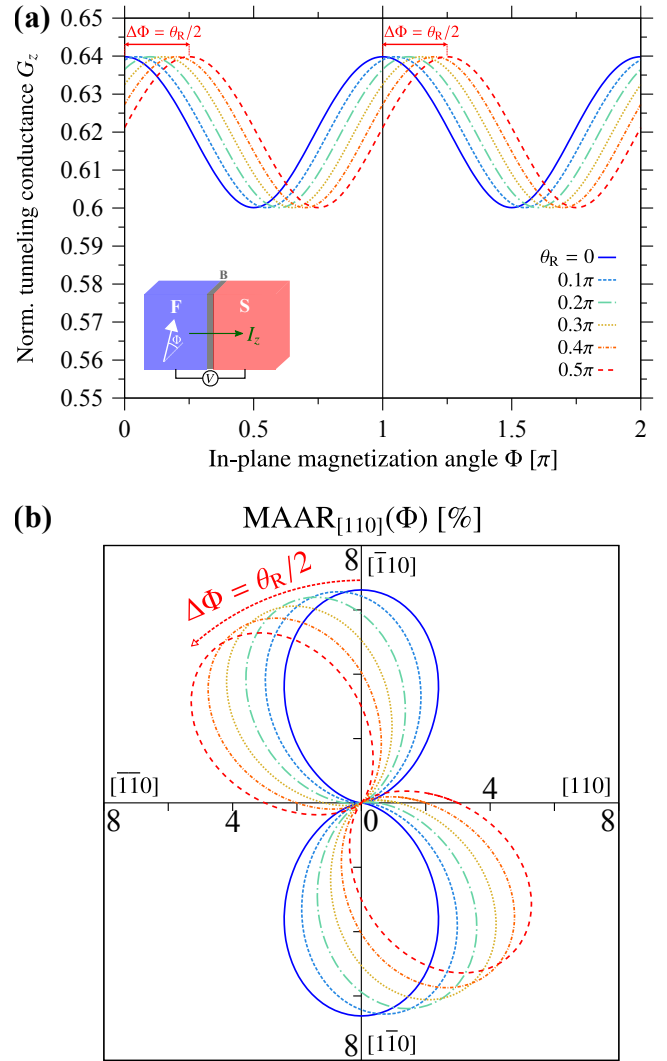


FIG. 3. (a) Calculated dependence of the tunneling conductance $G_z = dI_z/dV$ —normalized to Sharvin’s conductance $G_S = Ae^2k_F^2/(2\pi h)$ —on the in-plane magnetization angle Φ for various indicated Rashba angles $\theta_R \in [0; 0.5\pi]$; the Rashba (Dresselhaus) SOC parameters are $\lambda_R = 2m\alpha/\hbar^2 = 1$ ($\lambda_D = 2m\beta/\hbar^2 = 0.1 \ll \lambda_R$). (b) Angular dependence of the in-plane MAAR, evaluated according to Eq. (14).

to the preferred spin orientation (magnetization direction) in the ferromagnet—maximizing the probabilities for spin-flip scattering owing to the torque that acts on incoming electrons’ spins—and minimal if both are (anti)parallel. For CR SOC ($\theta_R = 0$), this results in maximal (minimal) conductance for in-plane magnetization angles $\Phi = 0 \bmod \pi$ ($\Phi = 0.5\pi \bmod \pi$), whereas RR SOC ($\theta_R = 0.5\pi$) requires $\Phi = 0.25\pi \bmod \pi$ ($\Phi = 0.75\pi \bmod \pi$); recall the orientation of the corresponding spin-orbit fields relative to the magnetization direction shown in Figs. 1(d) and 1(f). A general admixture of CR and RR SOC, quantified by the Rashba angle θ_R , imprints thus an overall $\Delta\Phi = \theta_R/2$ -shift on the angular dependence of the in-plane conductance magnetoanisotropy that is even more clearly evident when investigating the in-plane MAAR [74],

which is computed from

$$\text{MAAR}_{[110]}(\Phi) = \left. \frac{G_z(\Theta, \theta_R/2) - G_z(\Theta, \Phi)}{G_z(\Theta, \Phi)} \right|_{\Theta=0.5\pi} \quad (14)$$

and shown in Fig. 3(b).

B. Tunneling Anomalous Hall Effect

How to distinguish RR from CR SOC in the absence of Dresselhaus SOC? We previously proposed that spin- and transverse-momentum-dependent skew scattering (filtering) of incoming spin-polarized electrons at SOC-inducing barriers additionally rises a TAHE response, which is sizable in magnitude in superconducting junctions owing to a constructive interference of skew specular and Andreev reflections [47]. In contrast to the above-studied tunneling conductance, the TAHE is of first order in SOC and reflects a nontrivial dependence on the in-plane magnetization angle Φ already if only Rashba spin-orbit fields alone are present [4]. The non-collinear spin quantization axes, arising from the interplay of magnetization and spin-orbit fields, cause the in-plane magnetoanisotropy of the TAHE.

The following qualitative argument [4, 47] elucidates the mechanism of this magnetoanisotropy. For a fixed \mathbf{k}_{\parallel} -channel, the two preferred spatial directions in the junction are defined by the magnetization direction $\hat{\mathbf{m}}$ and the spin-orbit field $\hat{\mathbf{\Omega}}(\mathbf{k}_{\parallel})$. We can therefore expand the scattering-reflection-dependent part of the TAHE-conductance formula, Eq. (13), into the power series

$$G_{x(y)} \approx \frac{G_S}{2\pi k_F^2} \sum_{\sigma} \sum_{n=1}^{\infty} \int d^2\mathbf{k}_{\parallel} \frac{k_{x(y)}}{k_e^{\sigma}} c_n^{\sigma} [\hat{\mathbf{m}} \cdot \hat{\mathbf{\Omega}}(\mathbf{k}_{\parallel})]^n \quad (15)$$

with (in general complex) expansion coefficients c_n^{σ} . Scrutinizing the parity of the \mathbf{k}_{\parallel} -integrand, we conclude that both $G_{x(y)}$ are in first order approximated by the power-series contribution for $n = 1$ (the contribution for $n = 0$ vanishes due to parity), yielding

$$G_x \propto -\alpha \sin(\Phi - \theta_R) \quad (16)$$

and

$$G_y \propto \alpha \cos(\Phi - \theta_R) \quad (17)$$

for the in-plane magnetization-angle dependence of the TAHE conductances. Note that this result generalizes our findings in Ref. [47], in which only CR SOC was present corresponding to $\theta_R = 0$. *Probing the anisotropy of the TAHE conductances under in-plane magnetization rotations is thus predicted to enable determination of θ_R even in the absence of in-plane spin-orbit anisotropies.*

We wish to emphasize that similar physics arises also in normal-conducting junctions, for which first experiments have already successfully probed the TAHE in nanogranular films [13]; the advantage of superconducting junctions is that

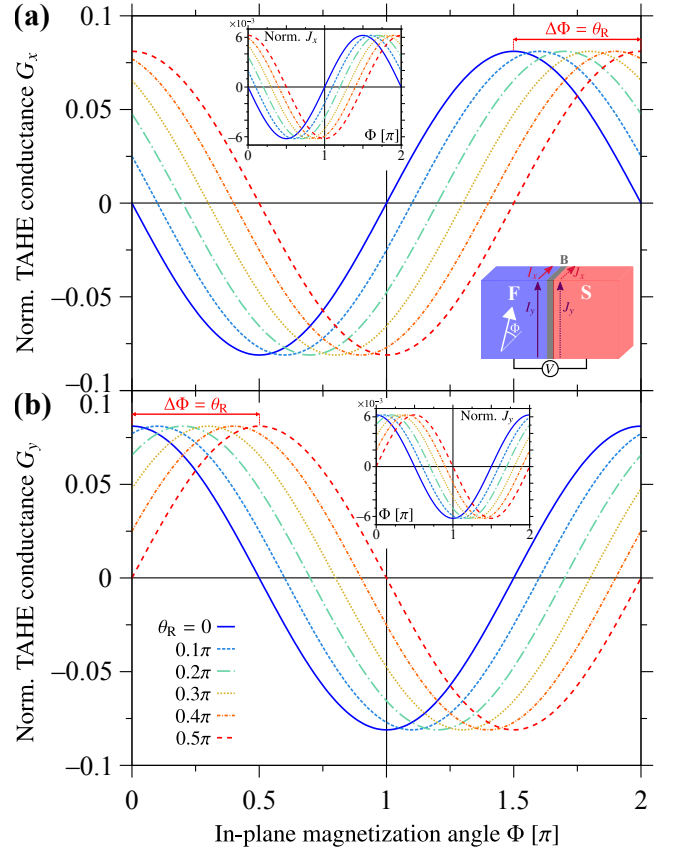


FIG. 4. Calculated TAHE conductances (a) $G_x = dI_x/dV$ and (b) $G_y = dI_y/dV$ —normalized to Sharvin’s conductance $G_S = Ae^2 k_F^2 / (2\pi h)$ —as functions of the in-plane magnetization angle Φ and for various indicated Rashba angles $\theta_R \in [0; 0.5\pi]$ at Rashba SOC $\lambda_R = 2ma/\hbar^2 = 1$; Dresselhaus SOC is absent. The insets show the corresponding Hall supercurrent responses J_x and J_y , computed in the superconductor and given in multiples of $\pi\Delta_0 G_S/e$.

additional skew Andreev reflections substantially enhance the TAHE and produce a more robust signal, in agreement with our numerical simulations.

Figure 4 presents the TAHE conductances G_x and G_y as functions of the in-plane magnetization angle Φ and for different Rashba angles $\theta_R \in [0; 0.5\pi]$. Both TAHE conductances reflect the Φ -dependencies that we deduced from parity arguments with the $\Delta\Phi = \theta_R$ -shifts at general θ_R . The maximal amplitudes of the TAHE conductances are independent of θ_R , as we assumed the same SOC amplitude α for CR- and RR-SOC contributions. Since there is no Dresselhaus SOC to interfere with, the *maximal* TAHE conductances are not subject to any crystallographic anisotropy, and their magnitudes are equal along the \hat{x} - and \hat{y} -directions. Moreover, we note the sizable amplitudes of the TAHE conductances (reaching nearly 10% of the respective tunneling conductance) due to the aforementioned skew Andreev reflections in the superconducting state; in the normal state, our calculations yield similar physics (i.e., the same $\Delta\Phi = \theta_R$ -shifts from that the Rashba angle can be experimentally extracted), but the absolute amplitudes of G_x and G_y are up to two orders of magnitude smaller

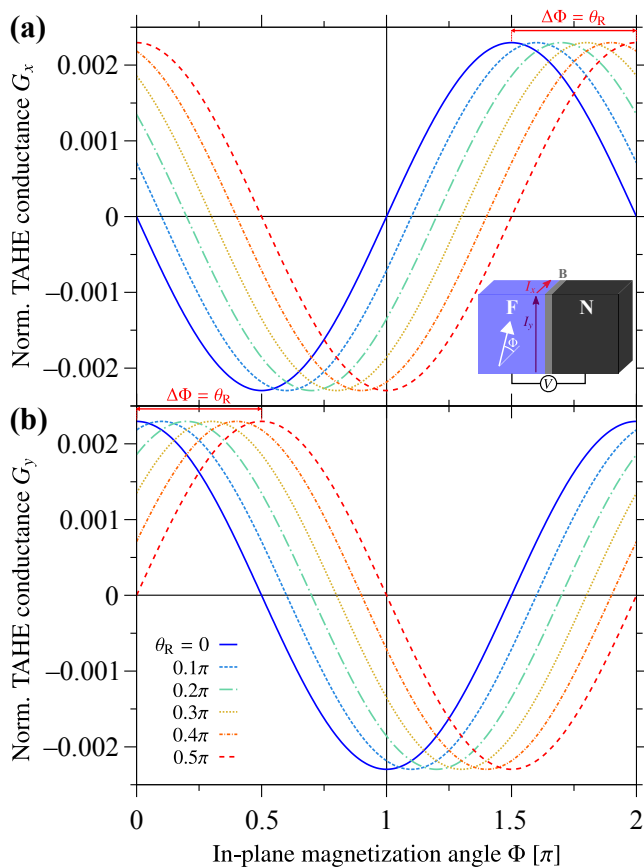


FIG. 5. Calculated *normal-state* (corresponding to the large-bias limit $eV \gg \Delta_0$) TAHE conductances (a) $G_x = dI_x/dV$ and (b) $G_y = dI_y/dV$ —normalized to Sharvin’s conductance $G_S = Ae^2k_F^2/(2\pi h)$ —as functions of the in-plane magnetization angle Φ and for various indicated Rashba angles $\theta_R \in [0, 0.5\pi]$ at Rashba SOC $\lambda_R = 2m\alpha/\hbar^2 = 1$; Dresselhaus SOC is absent.

(and less than 1 % of the respective tunneling conductance) as shown in Fig. 5, respectively.

As we demonstrated in Ref. [47], the skew Andreev-reflection process cycles Cooper pairs to the superconducting side of the junction, which are undergoing the spin- and transverse-momentum-dependent filtering as well, and trigger Hall supercurrent responses, denoted by J_x and J_y . The Φ -dependencies of J_x and J_y , calculated from our model as outlined in Appendix A and presented in the insets of Fig. 4, show the same $\Delta\Phi = \theta_R$ -shifts as the TAHE conductances, which convinces that both phenomena are indeed closely connected and result from the same skew-scattering mechanism.

Another advantage of the detection of RR SOC through TAHE measurements is the possibility to still disentangle its contribution from Dresselhaus SOC in situations in that also the latter is relevant. While RR and Dresselhaus spin-orbit fields have been predicted to manifest in the same magneto-transport and supercurrent-diode-effect characteristics in lateral (graphene-based) heterostructures [59]—owing to their coupling to the wave vector parallel to the tunneling current, which is similar for RR and Dresselhaus components—their

coupling to wave vectors perpendicular to the tunneling direction gives rise to well-distinct ramifications in the vertical junctions considered in this work. Generalizing the parity arguments from above allowing also for nonzero Dresselhaus SOC (parameterized by β), we obtain

$$G_x \propto -\alpha \sin(\Phi - \theta_R) - \beta \sin(\Phi) \quad (18)$$

and

$$G_y \propto \alpha \cos(\Phi - \theta_R) - \beta \cos(\Phi). \quad (19)$$

The θ_R -shift of G_x (G_y) is therefore fully induced by the RR component alone, while Dresselhaus SOC produces mainly an “offset” with the usual sinusoidal (co-sinusoidal) magnetization-angle dependence. As shown in Fig. 6 for purely RR SOC ($\theta_R = 0.5\pi$), the θ_R -shifts—and thereby the presence of RR SOC—are clearly resolvable from the TAHE data even for Dresselhaus parameters approaching the strength of the Rashba SOC ($\beta \rightarrow \alpha$); the amplitudes of the shifts are, however, suppressed with stronger Dresselhaus SOC as the non-shifted sin (cos) terms start to dominate producing higher-harmonic terms in the total TAHE conductances. Only if $\beta \gg \alpha$ —which is extremely unlikely for the considered systems as mentioned before—the θ_R -shifts (completely) disappear and the TAHE conductances are not conclusive to identify RR SOC. The *maximal* amplitudes of the TAHE conductances are remarkably damped at strong total SOC, as the SOC terms in the deltalike model additionally enhance interfacial scattering (reduce the transparency of the interface). The behavior of the Hall supercurrent responses J_x and J_y in the simultaneous presence of RR and Dresselhaus SOC (see the insets of Fig. 6) is qualitatively similar to the TAHE conductances. However, we note that the higher-harmonic terms stemming from the interference of the shifted RR and non-shifted Dresselhaus contributions are more pronounced in the Hall supercurrents and that the amplitudes of $J_{x(y)}$ initially remarkably increase with stronger Dresselhaus (before the final suppression due to the aforementioned additional scattering at the interface). The latter observation might be a possible indication of rather sizable triplet components in the Hall supercurrents.

IV. CONCLUSIONS

In summary, we applied well-established theoretical frameworks to investigate the magnetoanisotropies of the tunneling- and TAHE-conductance spectra of F/B/S junctions in the simultaneous presence of CR and unconventional RR SOC at the interface formed by a thin tunneling barrier (realized, e.g., through a twisted van-der-Waals bilayer). We demonstrated that a finite Rashba angle θ_R imprints a $\Delta\Phi = \theta_R$ -shift on the in-plane magnetization-angle dependence of the TAHE conductances in the ferromagnetic electrode, as well as on the corresponding Hall supercurrent responses in the superconductor, from which θ_R could be quantified in Hall-transport experiments. Both the out-of-plane and in-plane tunneling conductances, however, have been shown to be invariant of

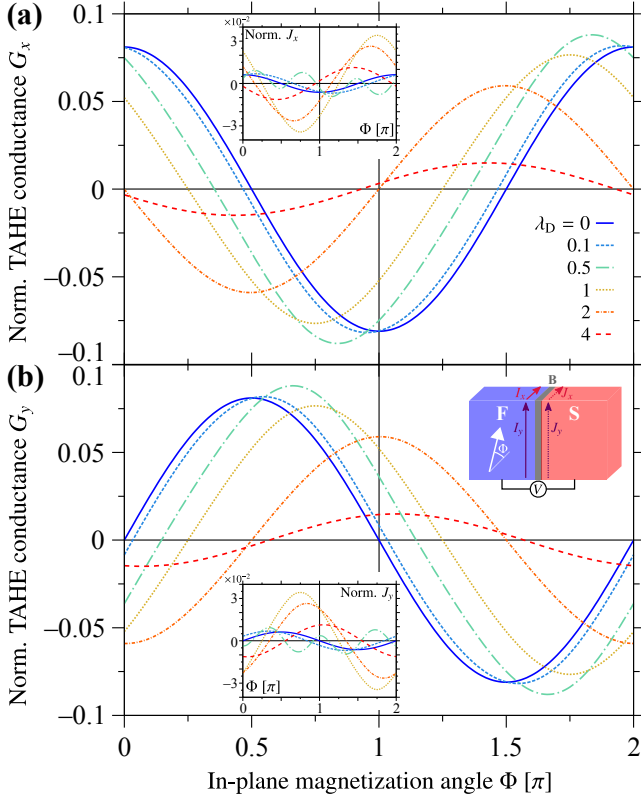


FIG. 6. Calculated TAHE conductances (a) $G_x = dI_x/dV$ and (b) $G_y = dI_y/dV$ —normalized to Sharvin’s conductance $G_S = Ae^2k_F^2/(2\pi h)$ —as functions of the in-plane magnetization angle Φ at purely RR SOC of strength $\lambda_R = 2m\alpha/\hbar^2 = 1$ ($\theta_R = 0.5\pi$) interfering with various indicated Dresselhaus SOC $\lambda_D = 2m\beta/\hbar^2$. The insets show the corresponding Hall supercurrent responses J_x and J_y , computed in the superconductor and given in multiples of $\pi\Delta_0G_S/e$.

θ_R if only Rashba SOC alone is present (as it is so far believed to be the case in twisted van-der-Waals bilayers) and only provide a distinction between CR and RR SOC when interfering with another, functionally distinct, spin-orbit field of, e.g., the Dresselhaus type. Studying tunneling-conductance magnetoanisotropies is thus nevertheless still an important experimental step to explicitly exclude possible Dresselhaus SOC in junctions with van-der-Waals barriers although the presence of weak Dresselhaus SOC would only have a minor impact on the θ_R -shifts of the TAHE conductances.

Appendix A: Calculation of the Hall supercurrent responses

To calculate the Hall supercurrent responses on the superconducting side, we adapt the Furusaki–Tsukada [75] Green’s-function approach similarly to Ref. [47]. For simplicity, we assume that the superconducting region spans the $z < 0$ -half space, while the ferromagnet is located at $z > 0$. Analogously to our formulation in the main text, the Bogoljubov–de Gennes

Hamiltonian can then be written as

$$\hat{\mathcal{H}}_{\text{BdG}} = \begin{bmatrix} \hat{\mathcal{H}}_e & \Delta_0 \Theta(-z) \hat{\sigma}_0 \\ \Delta_0 \Theta(-z) \hat{\sigma}_0 & -\hat{\sigma}_y \hat{\mathcal{H}}_e^* \hat{\sigma}_y \end{bmatrix} \quad (\text{A1})$$

with the single-electron Hamiltonian

$$\hat{\mathcal{H}}_e = \left(-\frac{\hbar^2}{2m} \nabla^2 - \mu \right) \hat{\sigma}_0 - \frac{\Delta_{\text{XC}}}{2} \Theta(z) (\hat{\mathbf{m}} \cdot \hat{\sigma}) + \hat{\mathcal{H}}_B; \quad (\text{A2})$$

the interface is described by

$$\hat{\mathcal{H}}_B = \left\{ V_B d_B \hat{\sigma}_0 + \alpha \left[\cos(\theta_R) (k_y \hat{\sigma}_x - k_x \hat{\sigma}_y) + \sin(\theta_R) (k_x \hat{\sigma}_x + k_y \hat{\sigma}_y) \right] - \beta (k_y \hat{\sigma}_x + k_x \hat{\sigma}_y) \right\} \delta(z), \quad (\text{A3})$$

accounting for the tunneling barrier with height (width) V_B (d_B), CR and RR SOC (strength α and Rashba angle θ_R), as well as Dresselhaus SOC (strength β).

The general solution of the Bogoljubov–de Gennes equation $\hat{\mathcal{H}}_{\text{BdG}} \Psi^{(1)}(\mathbf{r}) = E \Psi^{(1)}(\mathbf{r})$ for an incoming (1) spin-up electronlike quasiparticle from the superconductor is found to read as

$$\Psi^{(1)}(\mathbf{r}) = \psi^{(1)}(z) e^{i(k_x x + k_y y)}, \quad (\text{A4})$$

where

$$\begin{aligned} \psi^{(1)}(z < 0) = & e^{iq_e z} \begin{bmatrix} u \\ 0 \\ v \\ 0 \end{bmatrix} + \mathcal{A}^{(1)} e^{-iq_e z} \begin{bmatrix} u \\ 0 \\ v \\ 0 \end{bmatrix} + \mathcal{B}^{(1)} e^{-iq_e z} \begin{bmatrix} 0 \\ u \\ 0 \\ v \end{bmatrix} \\ & + \mathcal{C}^{(1)} e^{iq_h z} \begin{bmatrix} v \\ 0 \\ u \\ 0 \end{bmatrix} + \mathcal{D}^{(1)} e^{iq_h z} \begin{bmatrix} 0 \\ v \\ 0 \\ u \end{bmatrix} \end{aligned} \quad (\text{A5})$$

and

$$\begin{aligned} \psi^{(1)}(z > 0) = & \mathcal{E}^{(1)} e^{ik_c^{\sigma=1} z} \frac{1}{\sqrt{2}} \begin{bmatrix} \sqrt{1 + \cos(\Theta)} e^{-i\Phi} \\ \sqrt{1 - \cos(\Theta)} \\ 0 \\ 0 \end{bmatrix} \\ & + \mathcal{F}^{(1)} e^{ik_c^{\sigma=-1} z} \frac{1}{\sqrt{2}} \begin{bmatrix} -\sqrt{1 - \cos(\Theta)} e^{-i\Phi} \\ \sqrt{1 + \cos(\Theta)} \\ 0 \\ 0 \end{bmatrix} \\ & + \mathcal{G}^{(1)} e^{-ik_h^{\sigma=-1} z} \frac{1}{\sqrt{2}} \begin{bmatrix} 0 \\ 0 \\ \sqrt{1 + \cos(\Theta)} e^{-i\Phi} \\ \sqrt{1 - \cos(\Theta)} \end{bmatrix} \\ & + \mathcal{H}^{(1)} e^{-ik_h^{\sigma=1} z} \frac{1}{\sqrt{2}} \begin{bmatrix} 0 \\ 0 \\ -\sqrt{1 - \cos(\Theta)} e^{-i\Phi} \\ \sqrt{1 + \cos(\Theta)} \end{bmatrix}; \end{aligned} \quad (\text{A6})$$

the Bardeen–Cooper–Schrieffer coherence factors u and v are given by Eq. (7), and the spin- σ wave vectors within Andreev approximation ($E, \Delta_0 \ll \mu$) by Eqs. (8) and (9), respectively.

The scattering states $\Psi^{(2)}(\mathbf{r})$, $\Psi^{(3)}(\mathbf{r})$, and $\Psi^{(4)}(\mathbf{r})$ for incident (2) spin-down electronlike, (3) spin-up holelike, and (4) spin-down holelike quasiparticles are obtained in an analogous manner. The calligraphically written scattering coefficients are numerically determined applying interfacial ($z = 0$) boundary conditions as stated in Eqs. (10)–(11) and solving the resulting linear systems of equations. Particularly relevant are the spin-conserving Andreev-reflection coefficients $C^{(1)}$, $\mathcal{D}^{(2)}$, $\mathcal{A}^{(3)}$, and $\mathcal{B}^{(4)}$, which provide the input to calculate the Hall supercurrent responses close to the interface from [47]

$$J_{x(y)} = \frac{\pi\Delta_0 G_S}{e} \frac{k_B T}{2\pi k_F^2} \int d^2\mathbf{k}_{\parallel} \sum_{\omega_n} \frac{k_{x(y)}}{\sqrt{k_F^2 - \mathbf{k}_{\parallel}^2}} \times \left[\frac{C^{(1)}(i\omega_n) + \mathcal{D}^{(2)}(i\omega_n) + \mathcal{A}^{(3)}(i\omega_n) + \mathcal{B}^{(4)}(i\omega_n)}{\sqrt{\omega_n^2 + \Delta_0^2}} \right], \quad (\text{A7})$$

$k_B T$ is the thermal energy at temperature T (we finally consider $T/T_c = 0.1$, where T_c is the critical temperature of the superconductor) and $\omega_n = (2n + 1)\pi k_B T$, with integer n , are the fermionic Matsubara frequencies.

ACKNOWLEDGMENTS

A.C. and J.F. gratefully acknowledge funding by Deutsche Forschungsgemeinschaft (DFG; German Research Foundation) within the Research grant ‘‘Spin and magnetic properties of superconducting tunnel junctions’’ (Project-ID 454646522) and the Collaborative Research Center SFB 1277 (Project-ID 314695032, subproject B07).

-
- [1] I. Žutić, J. Fabian, and S. Das Sarma, *Rev. Mod. Phys.* **76**, 323 (2004).
- [2] J. Fabian, A. Matos-Abiague, C. Ertler, P. Stano, and I. Žutić, *Acta Phys. Slovaca* **57**, 565 (2007).
- [3] A. Matos-Abiague and J. Fabian, *Phys. Rev. B* **79**, 155303 (2009).
- [4] A. Matos-Abiague and J. Fabian, *Phys. Rev. Lett.* **115**, 056602 (2015).
- [5] P. Högl, A. Matos-Abiague, I. Žutić, and J. Fabian, *Phys. Rev. Lett.* **115**, 116601 (2015); *Phys. Rev. Lett.* **115**, 159902(E) (2015).
- [6] A. Costa, P. Högl, and J. Fabian, *Phys. Rev. B* **95**, 024514 (2017).
- [7] T. Vezin, C. Shen, J. E. Han, and I. Žutić, *Phys. Rev. B* **101**, 014515 (2020).
- [8] Y. A. Bychkov and E. I. Rashba, *J. Phys. C* **17**, 6039 (1984).
- [9] Y. A. Bychkov and E. I. Rashba, *Pis'ma Zh. Eksp. Teor. Fiz.* **39**, 66 (1984); *JETP Lett.* **39**, 78 (1984).
- [10] M. Gmitra, A. Matos-Abiague, C. Draxl, and J. Fabian, *Phys. Rev. Lett.* **111**, 036603 (2013).
- [11] G. Dresselhaus, *Phys. Rev.* **100**, 580 (1955).
- [12] J. Moser, A. Matos-Abiague, D. Schuh, W. Wegscheider, J. Fabian, and D. Weiss, *Phys. Rev. Lett.* **99**, 056601 (2007).
- [13] V. V. Rylkov, S. N. Nikolaev, K. Y. Chernoglazov, V. A. Demin, A. V. Sitnikov, M. Y. Presnyakov, A. L. Vasiliev, N. S. Perov, A. S. Vedenev, Y. E. Kalinin, V. V. Tugushev, and A. B. Granovsky, *Phys. Rev. B* **95**, 144202 (2017).
- [14] W. Han, R. K. Kawakami, M. Gmitra, and J. Fabian, *Nat. Nanotechnol.* **9**, 794 (2014).
- [15] I. Žutić, A. Matos-Abiague, B. Scharf, H. Dery, and K. Belashchenko, *Mater. Today* **22**, 85 (2019).
- [16] A. Avsar, H. Ochoa, F. Guinea, B. Özyilmaz, B. J. van Wees, and I. J. Vera-Marun, *Rev. Mod. Phys.* **92**, 021003 (2020).
- [17] J. F. Sierra, J. Fabian, R. K. Kawakami, S. Roche, and S. O. Valenzuela, *Nat. Nanotechnol.* **16**, 856 (2021).
- [18] D. T. Perkins and A. Ferreira, ‘‘Spintronics in 2D graphene-based van der Waals heterostructures,’’ in *Encyclopedia of Condensed Matter Physics*, edited by T. Chakraborty (Academic Press, Oxford, 2024) pp. 205–222, 2nd ed.
- [19] M. Gmitra, D. Kochan, P. Högl, and J. Fabian, *Phys. Rev. B* **93**, 155104 (2016).
- [20] Y. Li and M. Koshino, *Phys. Rev. B* **99**, 075438 (2019).
- [21] A. David, P. Rakyta, A. Kormányos, and G. Burkard, *Phys. Rev. B* **100**, 085412 (2019).
- [22] T. Naimer, K. Zollner, M. Gmitra, and J. Fabian, *Phys. Rev. B* **104**, 195156 (2021); *Phys. Rev. B* **108**, 039902 (2023).
- [23] C. G. Péterfalvi, A. David, P. Rakyta, G. Burkard, and A. Kormányos, *Phys. Rev. Res.* **4**, L022049 (2022).
- [24] A. Veneri, D. T. S. Perkins, C. G. Péterfalvi, and A. Ferreira, *Phys. Rev. B* **106**, L081406 (2022).
- [25] S. Lee, D. J. P. de Sousa, Y.-K. Kwon, F. de Juan, Z. Chi, F. Casanova, and T. Low, *Phys. Rev. B* **106**, 165420 (2022).
- [26] K. Zollner, P. E. Faria Junior, and J. Fabian, *Phys. Rev. B* **107**, 035112 (2023).
- [27] T. Naimer and J. Fabian, *Phys. Rev. B* **107**, 195144 (2023).
- [28] K. Zollner, S. M. João, B. K. Nikolić, and J. Fabian, *Phys. Rev. B* **108**, 235166 (2023).
- [29] T. Naimer, M. Gmitra, and J. Fabian, *Phys. Rev. B* **109**, 205109 (2024).
- [30] A. W. Cummings, J. H. Garcia, J. Fabian, and S. Roche, *Phys. Rev. Lett.* **119**, 206601 (2017).
- [31] T. S. Ghiasi, J. Ingla-Aynés, A. A. Kaverzin, and B. J. van Wees, *Nano Lett.* **17**, 7528 (2017).
- [32] S. Zihlmann, A. W. Cummings, J. H. Garcia, M. Kedves, K. Watanabe, T. Taniguchi, C. Schönenberger, and P. Makk, *Phys. Rev. B* **97**, 075434 (2018).
- [33] L. A. Benítez, J. F. Sierra, W. S. Torres, A. Arrighi, F. Bonell, M. V. Costache, and S. O. Valenzuela, *Nat. Phys.* **14**, 303 (2018).
- [34] G. Menichetti, L. Cavicchi, L. Lucchesi, F. Taddei, G. Iannaccone, P. Jarillo-Herrero, C. Felser, F. H. L. Koppens, and

- M. Polini, arXiv:2312.09169 (2023).
- [35] T. Frank, P. E. F. Junior, K. Zollner, and J. Fabian, *Phys. Rev. B* **109**, L241403 (2024).
- [36] M. Eschrig, *Phys. Today* **64**, 43 (2011).
- [37] J. Linder and J. W. A. Robinson, *Sci. Rep.* **5**, 15483 (2015).
- [38] F. S. Bergeret, A. F. Volkov, and K. B. Efetov, *Phys. Rev. Lett.* **86**, 4096 (2001).
- [39] A. F. Volkov, F. S. Bergeret, and K. B. Efetov, *Phys. Rev. Lett.* **90**, 117006 (2003).
- [40] R. S. Keizer, S. T. B. Goennenwein, T. M. Klapwijk, G. Miao, G. Xiao, and A. Gupta, *Nature (London)* **439**, 825 (2006).
- [41] K. Halterman, P. H. Barsic, and O. T. Valls, *Phys. Rev. Lett.* **99**, 127002 (2007).
- [42] M. Eschrig and T. Löfwander, *Nat. Phys.* **4**, 138 (2008).
- [43] K. Sun and N. Shah, *Phys. Rev. B* **91**, 144508 (2015).
- [44] A. Costa and J. Fabian, *Phys. Rev. B* **104**, 174504 (2021).
- [45] S. H. Jacobsen, I. Kulagina, and J. Linder, *Sci. Rep.* **6**, 23926 (2016).
- [46] I. Martínez, P. Högl, C. González-Ruano, J. P. Cascales, C. Tiusan, Y. Lu, M. Hehn, A. Matos-Abiague, J. Fabian, I. Žutić, and F. G. Aliev, *Phys. Rev. Appl.* **13**, 014030 (2020).
- [47] A. Costa, A. Matos-Abiague, and J. Fabian, *Phys. Rev. B* **100**, 060507(R) (2019).
- [48] F. Ando, Y. Miyasaka, T. Li, J. Ishizuka, T. Arakawa, Y. Shiota, T. Moriyama, Y. Yanase, and T. Ono, *Nature (London)* **584**, 373 (2020).
- [49] C. Baumgartner, L. Fuchs, A. Costa, S. Reinhardt, S. Gronin, G. C. Gardner, T. Lindemann, M. J. Manfra, P. E. Faria Junior, D. Kochan, J. Fabian, N. Paradiso, and C. Strunk, *Nat. Nanotechnol.* **17**, 39 (2022).
- [50] C. Baumgartner, L. Fuchs, A. Costa, J. Picó-Cortés, S. Reinhardt, S. Gronin, G. C. Gardner, T. Lindemann, M. J. Manfra, P. E. Faria Junior, D. Kochan, J. Fabian, N. Paradiso, and C. Strunk, *J. Phys. Condens. Matter* **34**, 154005 (2022).
- [51] A. Costa, C. Baumgartner, S. Reinhardt, J. Berger, S. Gronin, G. C. Gardner, T. Lindemann, M. J. Manfra, J. Fabian, D. Kochan, N. Paradiso, and C. Strunk, *Nat. Nanotechnol.* **18**, 1266 (2023).
- [52] A. Costa, J. Fabian, and D. Kochan, *Phys. Rev. B* **108**, 054522 (2023).
- [53] A. Banerjee, M. Geier, M. A. Rahman, C. Thomas, T. Wang, M. J. Manfra, K. Flensberg, and C. M. Marcus, *Phys. Rev. Lett.* **131**, 196301 (2023).
- [54] D. Kochan, A. Costa, I. Zhumagulov, and I. Žutić, arXiv:2303.11975 (2023).
- [55] S. Banerjee and M. S. Scheurer, *Phys. Rev. Lett.* **132**, 046003 (2024).
- [56] S. Banerjee and M. S. Scheurer, *Phys. Rev. B* **110**, 024503 (2024).
- [57] T. Kokkeler, I. Tokatly, and F. S. Bergeret, *SciPost Phys.* **16**, 055 (2024).
- [58] S. Reinhardt, T. Ascherl, A. Costa, J. Berger, S. Gronin, G. C. Gardner, T. Lindemann, M. J. Manfra, J. Fabian, D. Kochan, C. Strunk, and N. Paradiso, *Nat. Commun.* **15**, 4413 (2024).
- [59] W.-H. Kang, M. Barth, A. Costa, A. Garcia-Ruiz, A. Mreńca-Kolasińska, M.-H. Liu, and D. Kochan, *Phys. Rev. Lett.* **133**, 216201 (2024).
- [60] B. Scharf, D. Kochan, and A. Matos-Abiague, *Phys. Rev. B* **110**, 134511 (2024).
- [61] A. Costa, O. Kanehira, H. Matsueda, and J. Fabian, arXiv:2411.11570 (2024).
- [62] A. Daido, Y. Ikeda, and Y. Yanase, *Phys. Rev. Lett.* **128**, 037001 (2022).
- [63] N. F. Q. Yuan and L. Fu, *Proceedings of the National Academy of Sciences* **119**, e2119548119 (2022).
- [64] J. J. He, Y. Tanaka, and N. Nagaosa, *New Journal of Physics* **24**, 053014 (2022).
- [65] S. Ilić and F. S. Bergeret, *Phys. Rev. Lett.* **128**, 177001 (2022).
- [66] M. Davydova, S. Prembabu, and L. Fu, *Science Advances* **8**, eabo0309 (2022).
- [67] P. G. De Gennes, *Superconductivity of Metals and Alloys* (Addison Wesley, Redwood City, 1989).
- [68] F. Bonell, S. Andrieu, C. Tiusan, F. Montaigne, E. Snoeck, B. Belhadji, L. Calmels, F. Bertran, P. L. Fèvre, and A. Taleb-Ibrahimi, *Phys. Rev. B* **82**, 092405 (2010).
- [69] C. W. J. Beenakker, *Rev. Mod. Phys.* **69**, 731 (1997).
- [70] G. E. Blonder, M. Tinkham, and T. M. Klapwijk, *Phys. Rev. B* **25**, 4515 (1982).
- [71] For simplicity, the Hall-contact and interfacial cross-section areas are assumed to be equal and denoted by A .
- [72] A. Costa and J. Fabian, *Phys. Rev. B* **101**, 104508 (2020).
- [73] A. N. Chantis, K. D. Belashchenko, E. Y. Tsybal, and M. van Schilfgaarde, *Phys. Rev. Lett.* **98**, 046601 (2007).
- [74] Note that we generalized the formula for the in-plane MAAR stated in Ref. [5]. To obtain the maximal amplitudes of the magnetoanisotropy, the MAAR needs to be computed w.r.t. $G_z(\Theta, \theta_R/2)$, which corresponds to the maximal conductance at general Rashba angle θ_R as shown in Fig. 3(a). For CR SOC, $\theta_R = 0$ and the reference conductance is simply $G_z(\Theta, 0)$ as used in Ref. [5].
- [75] A. Furusaki and M. Tsukada, *Solid State Commun.* **78**, 299 (1991).